BRITISH JOURNAL OF HOSPITAL MEDICINE

ARTICLE

Ultrasound Radiomics for Preoperative Prediction of Cervical Lymph Node Metastasis in Medullary Thyroid Carcinoma

Quanhong Lu[1,2], Xiaoxia Zhu[2], Manman Li[3], Weiwei Zhan[4,*], Feng Feng[1,5,*]

[1]Imaging and Nuclear Medicine, Medical School of Nantong University, Nantong, Jiangsu, China
[2]Department of Ultrasound, Qidong People's Hospital & Qidong Liver Cancer Institute & Affiliated Qidong Hospital of Nantong University, Nantong, Jiangsu, China
[3]Department of Radiology, Yancheng NO.1 People's Hospital (The Fourth Affiliated Hospital of Nantong University), Yancheng, Jiangsu, China
[4]Department of Ultrasound, Ruijin Hospital, Shanghai Jiao Tong University School of Medicine, Shanghai, China
[5]Department of Radiology, Affiliated Tumour Hospital of Nantong University, Nantong, Jiangsu, China
*Correspondence: shanghairuijin@126.com (Weiwei Zhan); drfengfeng@163.com (Feng Feng)

Abstract

Aims/Background Medullary thyroid carcinoma (MTC) is a rare thyroid malignancy with a high mortality rate. Early detection of cervical lymph node metastasis (LNM) is critical for improving prognosis for patients with MTC. This study aimed to investigate the predictive utility of ultrasound-based radiomics for preoperative prediction of cervical LNM in MTC patients.

Methods The clinical, ultrasound, and pathological information of 193 patients with MTC were retrospectively examined. Radiomics features were obtained from the ultrasound images using PyRadiomics. The selected patients were randomly divided into training (n = 135) and validation (n = 58) cohorts. In the training dataset, radiomics features were selected using the least absolute shrinkage and selection operator (LASSO) regression, and the univariate and multivariate logistic regression tests were employed to identify the clinical independent predictors of cervical LNM. Three models were created: radiomics, clinical, and combined models, with the latter presented as a nomogram. The area under the curve (AUC) was calculated to evaluate the models' predictive performance. The differences in AUCs between the combined and approach-specific models were compared using the DeLong test. The clinical usefulness of the models was evaluated using decision curve analysis (DCA).

Results Nineteen radiomics features were chosen, and the AUCs of the developed radiomics model in the training and validation datasets were 0.881 and 0.859, respectively. Tumour diameter, calcitonin (Ctn) level, tumour margin, and sonographers' suspicion of cervical LNM based on ultrasound findings were clinical independent predictors for cervical LNM. The AUCs of the clinical model built using these predictors were 0.800 and 0.805 in the training and validation datasets, whereas the combined model had much-improved AUCs, measuring 0.925 for the training dataset and 0.918 for the validation test. The DeLong test indicated a significant AUC difference between the combined and clinical models (training dataset $p < 0.001$, validation dataset $p = 0.027$), but the difference between the combined and radiomics models was significant only in the training dataset (training dataset $p = 0.021$, validation dataset $p = 0.066$). Furthermore, based on the DCA results, the combined model features the largest clinical net benefit.

Conclusion The nomogram, the combined model merging the ultrasound-based radiomics with clinical independent predictors, effectively predicts preoperative cervical LNM in MTC patients, outperforming the radiomics and clinical models.

Key words: medullary thyroid carcinoma; radiomics; lymph node metastasis; nomogram

Submitted: 28 June 2024 Revised: 17 September 2024 Accepted: 23 September 2024

How to cite this article:
Lu Q, Zhu X, Li M, Zhan W, Feng F. Ultrasound Radiomics for Preoperative Prediction of Cervical Lymph Node Metastasis in Medullary Thyroid Carcinoma. Br J Hosp Med. 2025. https://doi.org/10.12968/hmed.2024.0376

Introduction

Medullary thyroid carcinoma (MTC) is a neuroendocrine tumour originating from the parafollicular cells (C cells) of the thyroid gland (Fugazzola, 2023). Although MTC accounts for only 5%–8% of all thyroid malignancies (Thomas et al, 2019), this tumour type has disproportionately contributed to 8.6%–13.4% of all deaths related to thyroid cancer (Duval et al, 2023; Konstantinidis et al, 2017). Studies have shown a strong correlation of cervical lymph node metastasis (LNM) with decreased survival rates and increased recurrence rates in MTC patients (Kandil et al, 2011; Siironen et al, 2016; Zhao et al, 2021). Based on a report, approximately 40.0%–66.7% of patients present with cervical LNM at the time of initial diagnosis (Fan et al, 2018).

At present, the extent of lymph node dissection (LND) required in the neck for MTC patients is still a matter of debate (Machens and Dralle, 2010; Wells et al, 2015), but the majority of surgeons lean towards a more comprehensive neck LND procedure (Randle et al, 2017). A study of 650 MTC patients revealed that 46.2% of patients underwent unnecessary neck LND (van Beek et al, 2021), and some reports also indicated that neck LND increases the risk of postoperative hypoparathyroidism, recurrent laryngeal nerve palsy, and lymphatic fistula, while incomplete lymph node (LN) clearance increases the risk of recurrence and reoperation (Baud et al, 2022; Hu and Ran, 2022; Kuo et al, 2018; Wu et al, 2021; Zhang et al, 2022). Therefore, early and accurate detection of LNM before surgery is crucial for reducing undertreatment or overtreatment in MTC patients. Currently, the assessment of cervical LNM in MTC patients mainly relies on cytological or histological analysis, which, although effective, carries risks such as bleeding and nerve injury. Additionally, the quality of the sample and the subjective judgment of the pathologist may also affect the accuracy of pathological analysis (Cui and Zhang, 2021; Li et al, 2021; Wang et al, 2023; Zhu et al, 2019).

Previous studies have shown that ultrasound-based radiomics of the primary lesion of thyroid cancer offer a noninvasive and effective strategy for predicting cervical LNM (Park et al, 2020; Shen et al, 2024; Wen et al, 2022). Currently, there are few studies using radiomics and ultrasound in tandem for the preoperative assessment of cervical LNM in MTC patients. Therefore, in this study, we aimed to construct a nomogram combining ultrasound-based radiomics with clinical independent predictors to noninvasively predict cervical LNM in MTC patients preoperatively.

Methods

Study Subjects

The current study was approved by the Ethics Committee of Ruijin Hospital, Shanghai Jiao Tong University School of Medicine (Ethics Review No.: 2024-320), and was conducted in accordance with the Declaration of Helsinki. Since this study was retrospective in nature, the ethics committee approved an exemption from the requirement to obtain informed consent from the patients or their guardians.

In this study, 193 patients who had been postoperatively, and pathologically diagnosed with MTC at Ruijin Hospital, Shanghai Jiao Tong University School of Medicine, from November 2012 to June 2022, were selected. Their historical ultrasound images along with pertinent clinical and pathological information were gathered for analysis. From the sample, there were 85 male and 108 female patients aged 13 to 78 years. The inclusion criteria for this study are as follows: (1) patients who were postoperatively, pathologically diagnosed with MTC; (2) patients with postoperative pathological results indicating whether LNM had occurred; (3) patients with preoperative thyroid and cervical lymph node ultrasound examination, having complete images and reports; and (4) lesions identified by ultrasound are consistent with those confirmed pathologically. The exclusion criteria are as follows: (1) patients with a history of thyroid surgery, ablation, radiotherapy, chemotherapy, or other tumour treatments; (2) patients with images of poor quality, which make effective analysis difficult; (3) patients with other malignant tumours or tumours in the thyroid, where it was not the primary site; and (4) patients with incomplete clinical and laboratory test data. Patients were randomly divided into two groups: a training cohort consisting of 135 individuals and a validation cohort comprising 58 individuals.

Ultrasound Examination

Owing to the extended duration involved in case selection and inclusion for this study, a variety of digital ultrasound imaging instruments from different brands and models were used, including:

- GE Healthcare's GE Logiq E8, probe model L6-15, manufactured in Wauwatosa, WI, USA.
- Philips Medical System's Philips HDI5, probe model L12-5, manufactured in Bothell, WA, USA.
- Esaote S.p.A.'s Esaote MYlab series, probe model L4-15, manufactured in Genoa, Italy.
- Mindray Medical International Limited's Mindray Resona series, including Resona7 and Resona9, probe models L14-5WU and L14-3Ws, manufactured in Shenzhen, China.
- Samsung Medison Co., Ltd.'s SAMSUNG RS80A, probe model L3-12A, manufactured in Seoul, South Korea.

During ultrasound examination, the patients were instructed to lay in a supine positioned with their heads tilted backward in order to fully expose the neck. Transverse and longitudinal scans of the neck area were performed using a 6–18 MHz ultrasound probe. The ultrasound evaluation criteria were referenced from the "2020 Chinese Guidelines for the Ultrasound Malignancy Risk Stratification of Thyroid Nodules" (Zhou et al, 2020), covering aspects such as tumour location, diameter, shape, multifocality, composition, echogenicity, echotexture, margin, posterior features, echogenic foci, vascularity, blood supply, sonographers' suspicion of cervical LNM based on ultrasound findings, and presence of diffuse thyroid disease.

Image Annotation and Feature Extraction

The longest axis of the thyroid nodule in the cross-section was chosen from each patient's ultrasound image. The image format was converted from JPG to NIfTI using onekey (version 2.1.12; OnekeyAI Platform, Beijing, China; https://github.com/OnekeyAI-Platform/onekey) and then uploaded to ITK-SNAP software (version 3.8.0; Penn Image Computing and Science Laboratory, University of Pennsylvania, Philadelphia, PA, USA; http://www.itksnap.org). The region of interest (ROI) was manually delineated independently by two sonographers (5 and 13 years of clinical experience, respectively). Without knowing the patient's clinical and pathological data, preprocessing of the ultrasound images was conducted, including grayscale and contrast adjustment. Then, the boundaries of the nodules were delineated in detail along the longest axis in the cross-section of the nodules, including the delineation of thyroid echogenicity changes around the nodules, while avoiding thyroid vessels and artifactual images. Finally, the tumour images and ROI masks were exported (Fig. 1a,b).

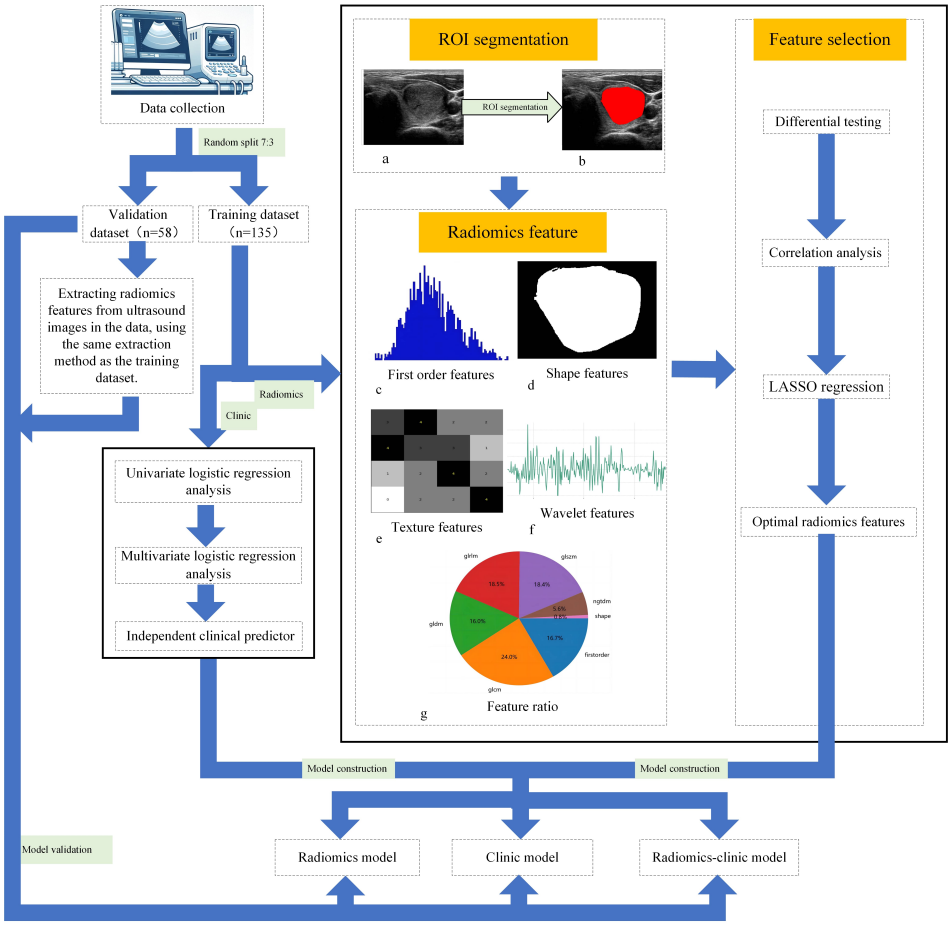

Fig. 1. Workflow of model construction. (a) Ultrasound imaging. (b) ROI segmentation of MTC. (c) First-order gray-level histogram features. (d) Shape features. (e) Texture features. (f) Wavelet features. (g) Ratio of radiomics features. Abbreviations: GLCM, gray-level co-occurrence matrix; GLDM, gray-level dependence matrix; GLRLM, gray-level run length matrix; GLSZM, gray-level size zone matrix; NGTDM, neighboring gray-tone difference matrix; ROI, region of interest; LASSO, least absolute shrinkage and selection operator; MTC, medullary thyroid carcinoma.

Radiomics features were extracted using PyRadiomics (version 3.0.1; Computational Imaging & Bioinformatics Lab, Harvard Medical School, Boston, MA, USA; https://pyradiomics.readthedocs.io) in Python (version 3.7.12; Python Software Foundation, Wilmington, DE, USA; https://www.python.org). These features included various attributes such as shape, texture, and intensity, with some feature types illustrated in Fig. 1c–f. The Z-score method was used to standardize these features, transforming the data to a mean of 0 and a standard deviation of 1.

Intra-Observer and Inter-Observer Consistency Assessment

Thirty ultrasound images of patients were randomly selected. Independently, two sonographers (5 and 13 years of clinical experience, respectively) defined the ROI and extracted radiomics features. Two weeks later, the more senior sonographer delineated the ROI and extracted radiomics features from the same images independently. The intra/inter-class correlation coefficient (ICC) was calculated to evaluate the intra-observer and inter-observer consistency of feature extraction. ICC >0.75 indicated a high level of consistency.

Feature Selection

Radiomics feature selection: In the training dataset, radiomics features standardized by Z-score were first subjected to differential testing, retaining features with $p < 0.05$. After that, a correlation analysis was performed, and only one feature was retained when two features had a correlation coefficient larger than 0.9 (Wang et al, 2021). Redundant features were further removed using the recursive feature elimination method. Finally, the least absolute shrinkage and selection operator (LASSO) regression model was used to select the optimal radiomics features based on the best regularization parameter λ. The radiomics score (Rad-score) for each patient was obtained by linearly combining the optimal radiomics features, with the weight of each feature being its coefficient in the LASSO regression model.

Clinical feature selection: A univariate logistic regression analysis of clinical features was performed, followed by a multivariate backward stepwise logistic regression analysis. Clinical features with $p < 0.05$ in the multivariate analysis were selected as the clinical independent predictors of cervical LNM in MTC patients.

Model Construction and Performance Evaluation

Radiomics model: The construction of radiomics model was executed using the logistic regression machine learning algorithm. The selected optimal radiomics features were applied to the radiomics model, generating the radiomics signature (i.e., the predicted probability of the radiomics model).

Clinical model: The construction of the model was conducted by employing the logistic regression machine learning algorithm. The clinical independent predictors were applied to the clinical model.

Combined model: The combined model was built by integrating the radiomics model and the clinical independent predictors. The results of the combined model were presented in the form of a nomogram.

The models' predicted outcomes were validated against the postoperative pathological outcomes of cervical LN. The predictive performance of these models was assessed using accuracy, area under the curve (AUC), sensitivity, specificity, positive predictive value (PPV), and negative predictive value (NPV). The cut-off values for each model were determined using the receiver operating characteristic (ROC) curve analysis on the training dataset, selecting the threshold that maximized Youden's J statistic (J = sensitivity + specificity – 1). To ensure consistency, the same cut-off values were applied to the validation dataset. To determine whether the variations in AUC between the combined model and the clinical model, and between the combined model and the radiomics model were statistically significant, the DeLong test was employed. Calibration curves were plotted to evaluate the calibration performance of the three models, and the Hosmer-Lemeshow test was used to analyze the goodness of fit between the predicted results of the three models and the actual occurrence. Decision curve analysis (DCA) was used to further explore the clinical application value of these predictive models.

Statistical Analysis

In the training dataset, the standardized radiomics features were tested for normality using the one-sample Kolmogorov-Smirnov test. Normally distributed features were analyzed with a two-sample *t*-test, while non-normal features were analyzed with the Mann-Whitney U test. For correlation analysis, the Pearson correlation coefficient was used if all features were normally distributed; otherwise, the Spearman rank correlation coefficient was used (Temizhan et al, 2022; van den Heuvel and Zhan, 2022). The chi-square test or Fisher's exact test was used to compare the differences in sensitivity, specificity, PPV, NPV, and accuracy between the radiomics, clinical and combined models.

For the analysis of clinical baseline data, the Shapiro-Wilk test was used to check the normality of continuous clinical variables. Normally distributed features are presented as mean ± standard deviation and were analyzed using a two-sample *t*-test. Non-normally distributed features are expressed as median (P25, P75) [M (P25, P75)] and analyzed with the Mann-Whitney U test. Nominal categorical variables were compared using the chi-square test.

Differential analyses (*t*-tests, U tests, chi-square tests, and Fisher's exact tests) of radiomic and clinical features, as well as univariate and multivariate logistic regression analyses, were conducted using Python (version 3.7.12; Python Software Foundation, Wilmington, DE, USA; https://www.python.org) and statsmodels (version 0.13.2; Statsmodels Developers; https://www.statsmodels.org) software. A *p*-value of less than 0.05 was deemed statistically significant. LASSO regression analysis, model development, and ROC curve analysis were performed using the scikit-learn package (version 1.0.2; scikit-learn developers; https://scikit-learn.org) in Python version 3.7.12. The DeLong test, DCA, and Hosmer-Lemeshow test were conducted using onekey (version 2.1.12; OnekeyAI Platform, Beijing, China; https://github.com/OnekeyAI-Platform/onekey).

Table 1. Clinical baseline characteristics of patients.

Feature name	Without LNM (n = 119)	With LNM (n = 74)	Z/χ^2	*p*-value
Age (years)	54.00 (39.50, 62.00)	49.00 (32.50, 58.00)	1.500	0.134
Tumour diameter (mm)	12.60 (8.10, 20.00)	19.30 (13.43, 30.78)	–4.365	<0.001*
Gender			3.653	0.056
Female	73 (61.34)	35 (47.30)		
Male	46 (38.66)	39 (52.70)		
Multifocality			4.427	0.035*
No	111 (93.28)	62 (83.78)		
Yes	8 (6.72)	12 (16.22)		
Tumour location 1			0.038	0.845
Left lobe	58 (48.74)	35 (47.30)		
Right lobe	61 (51.26)	39 (52.70)		
Tumour location 2			9.886	0.020*
Upper pole	30 (25.21)	24 (32.43)		
Inferior pole	15 (12.61)	5 (6.76)		
Middle pole	67 (56.30)	32 (43.24)		
Penetrating the medial and lateral aspects, or the ventral and dorsal aspects	7 (5.88)	13 (17.57)		
Cross-sectional shape			5.949	0.015*
Wider-than-tall	53 (44.54)	20 (27.03)		
Taller-than-wide	66 (55.46)	54 (72.97)		
Longitudinal section shape			3.144	0.076
Wider-than-tall	94 (78.99)	50 (67.57)		
Taller-than-wide	25 (21.01)	24 (32.43)		
Composition			0.316	0.574
Solid	79 (66.39)	52 (70.27)		
Cystic-solid mixed	40 (33.61)	22 (29.73)		
Echogenicity			8.355	0.015*
Hypoechoic	58 (48.74)	50 (67.57)		
Isoechoic	56 (47.06)	24 (32.43)		
Markedly hypoechoic	5 (4.20)	0 (0)		
Margin			20.060	<0.001*
Circumscribed	66 (55.46)	21 (28.38)		
Irregular margin	16 (13.45)	16 (21.62)		
Ill defined	33 (27.73)	24 (32.43)		
ETE	4 (3.36)	13 (17.57)		
Posterior features			6.611	0.037*
No posterior features	92 (77.31)	58 (78.38)		
Enhancement	14 (11.76)	2 (2.70)		
Shadowing due to macrocalcification	13 (10.92)	14 (18.92)		
Echogenic foci			14.590	0.002*
No echogenic foci	64 (53.78)	21 (28.38)		

Table 1. Continued.

Feature name	Without LNM (n = 119)	With LNM (n = 74)	Z/χ^2	*p*-value
Microcalcifications	32 (26.89)	38 (51.35)		
Macrocalcifications	10 (8.40)	8 (10.81)		
Microcalcifications and macrocalcifications	13 (10.92)	7 (9.46)		
Vascularity			1.416	0.493
Mainly central vascularity	2 (1.68)	0 (0)		
Mainly peripheral vascularity	38 (31.93)	22 (29.73)		
Mixed vascularity	79 (66.39)	52 (70.27)		
Echotexture			11.739	0.001*
Homogeneous	62 (52.10)	20 (27.03)		
Heterogeneous	57 (47.90)	54 (72.97)		
Blood supply			2.462	0.292
Poor	36 (30.25)	16 (21.62)		
Medium	30 (25.21)	17 (22.97)		
Rich	53 (44.54)	41 (55.41)		
Combined with diffuse thyroid disease			0.418	0.518
No	108 (90.76)	65 (87.84)		
Yes	11 (9.24)	9 (12.16)		
CEA			0.005	0.942
Negative	38 (31.93)	24 (32.43)		
Positive	81 (68.07)	50 (67.57)		
Ctn (pg/mL)			12.671	0.013*
<20	21 (17.65)	5 (6.76)		
20–50	6 (5.04)	3 (4.05)		
50–200	21 (17.65)	5 (6.76)		
200–500	14 (11.76)	8 (10.81)		
>500	57 (47.90)	53 (71.62)		
Sonographers' suspicion of cervical LNM based on ultrasound findings			29.541	<0.001*
No	86 (72.27)	24 (32.43)		
Yes	33 (27.73)	50 (67.57)		

Notes: * Differences are statistically significant. Age and tumour diameter were assessed using the Mann-Whitney U test, presented as M (P25, P75). Other features were assessed using the chi-square test, presented as frequency (%).
Abbreviations: ETE, extrathyroidal extension; CEA, Carcinoembryonic antigen; Ctn, calcitonin; LNM, lymph node metastasis.

Results

Selection of Clinical Independent Predictors

This study included 193 MTC patients, of whom 38.34% (74/193) were positive for cervical LNM, while 61.66% (119/193) were negative for cervical LNM. The results of the differential analysis of clinical features between MTC patients

with cervical LNM and without LNM showed that tumour diameter, multifocality, tumour location 2, cross-sectional shape, echogenicity, echotexture, margin, posterior features, echogenic foci, calcitonin (Ctn) level, and sonographers' suspicion of cervical LNM based on ultrasound findings had statistically significant differences between the two groups ($p < 0.05$), while the remaining features showed no statistical significance ($p > 0.05$), as detailed in Table 1. Multivariate backward stepwise logistic regression analysis showed that tumour diameter (odds ratio [OR]: 1.009, 95% confidence interval [CI]: 1.005–1.014, $p = 0.001$), Ctn (OR: 1.059, 95% CI: 1.020–1.100, $p = 0.013$), margin (OR: 1.091, 95% CI: 1.038–1.148, $p = 0.005$), and sonographers' suspicion of cervical LNM based on ultrasound findings (OR: 1.282, 95% CI: 1.155–1.425, $p < 0.001$) were clinical independent predictors of whether cervical LNM occurs in MTC patients (Table 2). Fig. 2 presents the correlation coefficient heatmap of the clinical independent predictors constructed based on the Spearman rank correlation coefficient.

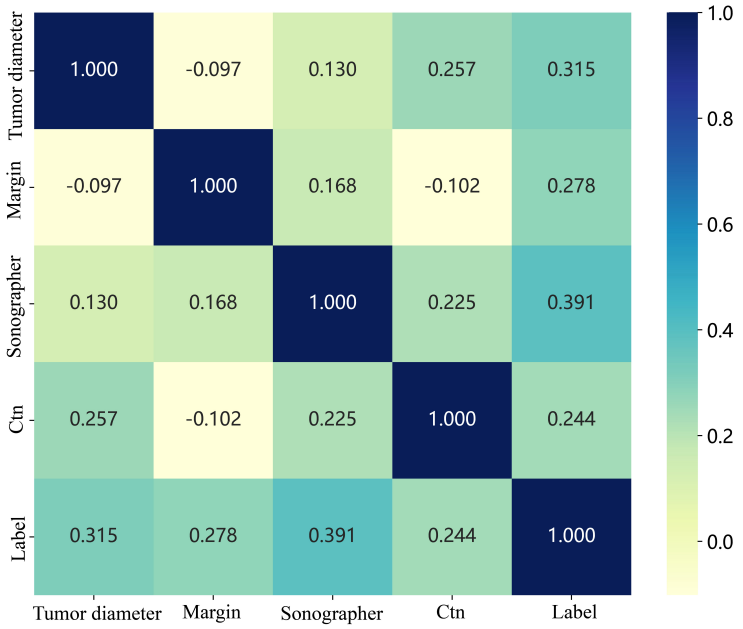

Fig. 2. Correlation coefficient heatmap of the clinical independent predictors.

Selection of Ultrasound Radiomics Features

A total of 1459 features were extracted for each individual ROI. The proportion of features is detailed in Fig. 1g. The intra-observer and inter-observer consistency were high, with ICC values exceeding 0.75. The results of the one-sample Kolmogorov-Smirnov test showed that some features did not follow a normal distribution.

In the training dataset, 463 features were retained after differential testing of radiomics features (Fig. 3). Subsequently, 102 features were further selected through Spearman rank correlation analysis and recursive feature elimination. Finally, 19 optimal radiomics features were screened using the LASSO regression model (Fig. 4

Table 2. Univariate logistic regression analysis and multivariate backward stepwise logistic regression analysis of the training dataset.

Feature name	Univariate logistic regression analysis (n = 135)				Multivariate backward stepwise logistic regression analysis (n = 135)			
	OR	Lower 95% CI	Upper 95% CI	*p*-value	OR	Lower 95% CI	Upper 95% CI	*p*-value
Echogenicity	0.834	0.752	0.926	0.004*	0.918	0.832	1.014	0.155
Composition	0.959	0.846	1.085	0.577				
Age	0.996	0.992	1.000	0.109				
CEA	0.995	0.878	1.126	0.943				
Tumour location 1	1.014	0.902	1.139	0.846				
Tumour location 2	1.012	0.976	1.049	0.580				
Tumour diameter	1.013	1.008	1.018	0.000*	1.009	1.005	1.014	0.001*
Vascularity	1.025	0.965	1.089	0.506				
Posterior features	1.033	0.952	1.120	0.515				
Echogenic foci	1.063	1.020	1.108	0.014*	1.029	0.991	1.068	0.207
Blood supply	1.067	0.996	1.143	0.119				
Ctn	1.081	1.040	1.124	0.001*	1.059	1.020	1.100	0.013*
Combined with diffuse thyroid disease	1.077	0.890	1.303	0.520				
Margin	1.138	1.079	1.201	0.000*	1.091	1.038	1.148	0.005*
Gender	1.144	1.019	1.285	0.056				
Longitudinal section shape	1.153	1.010	1.317	0.077				
Cross-sectional shape	1.192	1.060	1.342	0.015*	1.113	0.996	1.244	0.113
Echotexture	1.275	1.138	1.429	0.001*	1.050	0.933	1.181	0.493
Multifocality	1.273	1.054	1.537	0.036*	1.172	0.995	1.381	0.111
Sonographers' suspicion of cervical LNM based on ultrasound findings	1.468	1.318	1.636	0.000*	1.282	1.155	1.425	0.000*

Notes: * Differences are statistically significant.
Abbreviations: OR, odds ratio; CI, confidence interval.

Table 3. Comparison of prediction performance of clinical, radiomics and combined models in training and validation datasets.

Group	Training dataset			Validation dataset		
Model	Clinical model (cut-off: 0.494)	Radiomics model (cut-off: 0.479)	Combined model (cut-off: 0.252)	Clinical model (cut-off: 0.494)	Radiomics model (cut-off: 0.479)	Combined model (cut-off: 0.252)
Accuracy	0.785	0.822	0.844	0.776	0.793	0.828
p-value	0.210	0.624	-	0.641	0.813	-
AUC (95% CI)	0.800 (0.722–0.879)	0.881 (0.825–0.938)	0.925 (0.882–0.968)	0.805 (0.693–0.918)	0.859 (0.758–0.961)	0.918 (0.842–0.995)
p-value	0.000*	0.021*	-	0.027*	0.066	-
Sensitivity	0.667	0.778	0.944	0.500	0.800	0.850
p-value	<0.001*	0.024*	-	0.041*	1.000	-
Specificity	0.864	0.852	0.778	0.921	0.790	0.816
p-value	0.218	0.312	-	0.309	1.000	-
PPV	0.766	0.778	0.739	0.769	0.667	0.708
p-value	0.829	0.676	-	1.000	1.000	-
NPV	0.796	0.852	0.955	0.778	0.882	0.912
p-value	0.004*	0.055	-	0.136	1.000	-

Notes: * Differences are statistically significant. The *p*-value for comparing AUCs was calculated using the DeLong test. The *p*-values for comparing accuracy, sensitivity, specificity, PPV, and NPV were calculated using the chi-square test or Fisher's exact test.
Abbreviations: AUC, area under the curve; PPV, positive predictive value; NPV, negative predictive value.

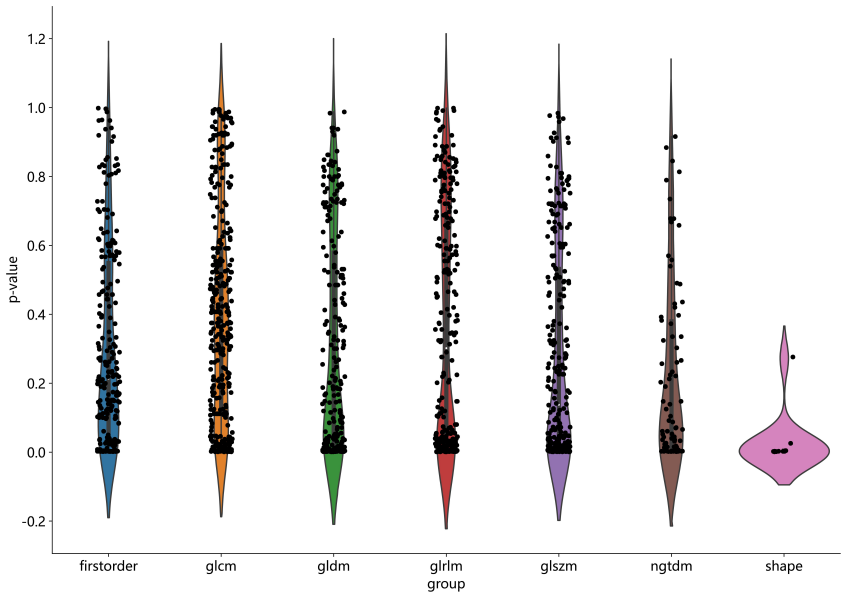

Fig. 3. Statistics of radiomic features.

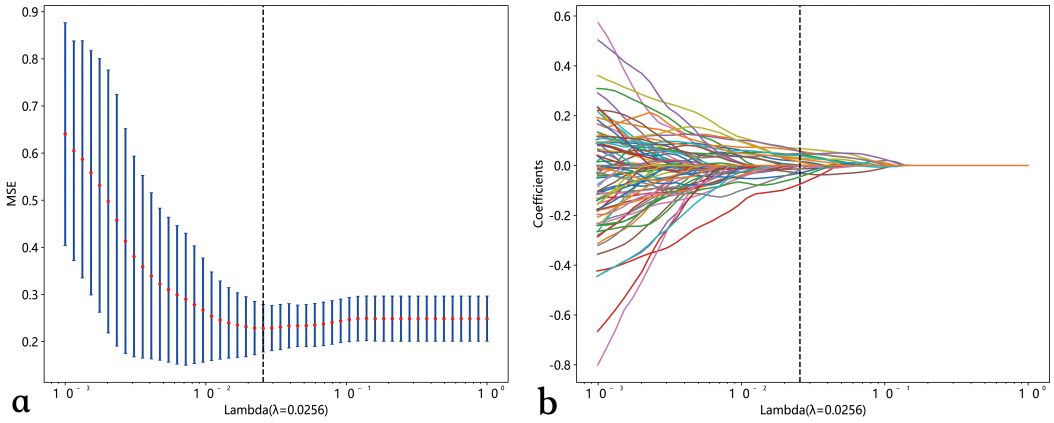

Fig. 4. LASSO regression model for selecting radiomics features. (a) LASSO regression 10-fold cross-validation plot. (b) LASSO regression coefficient plot. Abbreviations: MSE, Mean squared error.

a,b). The 19 optimal radiomics features and their coefficients are shown in Fig. 5. The following formula is employed to calculate the Rad-score:

Rad-score = 0.400000000000002 – 0.002934 × gradient_glcm_Imc2 – 0.075159 × lbp_3D_k_glszm_ZoneVariance – 0.030066 × lbp_3D_k_ngtdm_Contrast + 0.001773 × lbp_3D_m2_glszm_SizeZoneNonUniformity – 0.013494 × squareroot_ngtdm_Strength + 0.016174 × wavelet_HHH_glszm_SizeZoneNonUniformity + 0.067796 × wavelet_HLH_glrlm_LowGrayLevelRunEmphasis + 0.057640 × wavelet_HLH_glszm_SmallAreaHighGrayLevelEmphasis – 0.030168 × wavelet_HLL_glszm_LargeAreaHighGrayLevelEmphasis + 0.014861 × wavelet_HLL_glszm_LargeAreaLowGrayLevelEmphasis + 0.042752 × wavelet_HLL_glszm_SmallAreaHighGrayLevelEmphasis + 0.058420 × wavelet_HLL_ngtdm_Complexity – 0.000810 × wavelet_LHH_glcm_MaximumProbability + 0.047629 × w

avelet_LHH_gldm_LowGrayLevelEmphasis + 0.030788 × wavelet_LHH_glrlm_GrayLevelVariance + 0.040130 × wavelet_LHH_glszm_SizeZoneNonUniformity + 0.025317 × wavelet_LHH_glszm_SmallAreaHighGrayLevelEmphasis – 0.017284 × wavelet_LHL_ngtdm_Complexity – 0.045633 × wavelet_LLH_glrlm_RunPercentage.

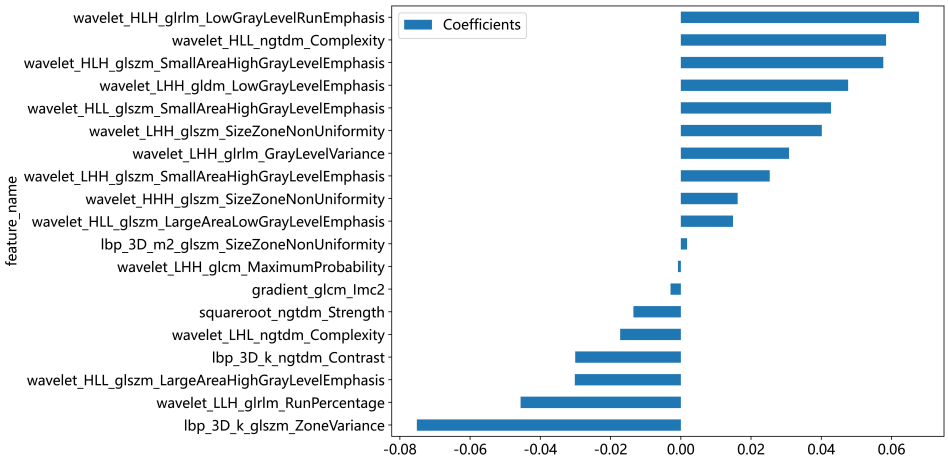

Fig. 5. Coefficient plot of 19 LASSO-selected radiomics features.

Performance Evaluation of Different Models

Models incorporating clinical data, radiomics, and their combination were constructed using logistic regression techniques. For the training dataset, the AUCs were as follows: 0.800 (95% CI: 0.722–0.879) for the clinical model, 0.881 (95% CI: 0.825–0.938) for the radiomics model, and 0.925 (95% CI: 0.882–0.968) for the combined model. Similarly, within the validation dataset, the AUCs were 0.805 (95% CI: 0.693–0.918) for the clinical model, 0.859 (95% CI: 0.758–0.961) for the radiomics model, and 0.918 (95% CI: 0.842–0.995) for the combined model. The details are presented in Table 3 and Fig. 6a,b.

As shown in Table 3, when comparing the combined model to the clinical model, the DeLong test revealed a statistically significant difference in AUC ($p = 0.027$ in the validation dataset and $p < 0.001$ in the training dataset). However, statistical significance was observed only in the training dataset ($p = 0.021$) and not in the validation dataset ($p = 0.066$) when comparing the AUCs of the combined model and the radiomics model. In the training dataset, the sensitivity of the combined model was higher than that of the clinical model and the radiomics model by 0.277 ($p < 0.001$) and 0.166 ($p = 0.024$), respectively, while the differences in specificity and PPV were not statistically significant. In the validation dataset, the sensitivity of the combined model was higher than that of the clinical model by 0.350 ($p = 0.041$), but the difference with the radiomics model was not statistically significant. Additionally, in the training dataset, the NPV of the combined model was significantly higher than that of the clinical model (0.955 vs. 0.796, $p = 0.004$).

The calibration curve analysis indicated that, among the three models, the combined model's predicted outcomes closely approached the actual outcomes in both

Table 4. Results of Hosmer-Lemeshow test across the three predictive models on the training and validation datasets.

Group	Clinical model	Radiomics model	Combined model
Training dataset	$p = 0.808$	$p = 0.245$	$p = 0.865$
Validation dataset	$p = 0.668$	$p = 0.824$	$p = 0.545$

the training and validation datasets by a high resemblance (Fig. 6c,d). The Hosmer-Lemeshow test revealed that the disparities between the predicted results and the actual occurrences in the training and validation datasets were not statistically significant ($p > 0.05$) for any of the three models (Table 4). DCA results indicated that all three models had clinical application value, with the combined model showing the largest clinical net benefit within specific threshold probability ranges (approximately 0–0.85 in the training dataset and 0.13–1.00 in the validation dataset). The details are shown in Fig. 6e,f.

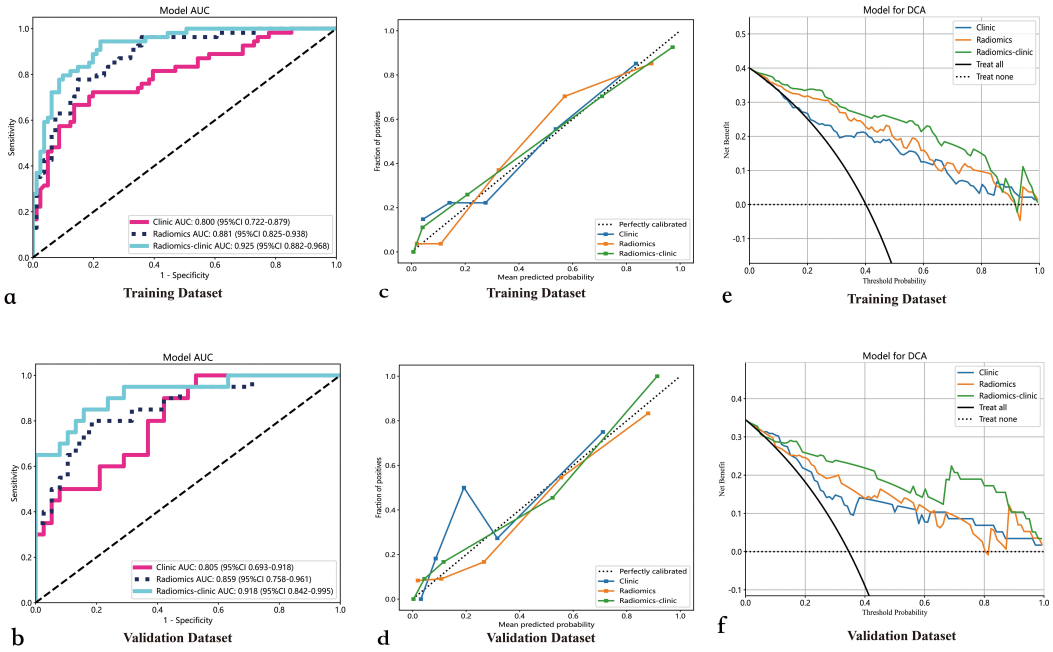

Fig. 6. Performance evaluation of models for predicting cervical LNM in MTC. (a,b) ROC curves of clinical, radiomics and combined models for predicting cervical LNM in MTC: training (a) and validation datasets (b). (c,d) Calibration curves of clinical, radiomics and combined models for cervical LNM prediction in MTC: training (c) and validation datasets (d). (e,f) Decision curve analysis of clinical, radiomics and combined models for predicting cervical LNM in MTC: training (e) and validation datasets (f). Abbreviations: LNM, lymph node metastasis; MTC, medullary thyroid carcinoma; ROC, receiver operating characteristics.

Nomogram for the Combined Model

Fig. 7 illustrates the nomogram constructed based on the combined model. Two cases were randomly selected as examples to demonstrate application of the nomogram in formulating personalized treatment plans (Fig. 8).

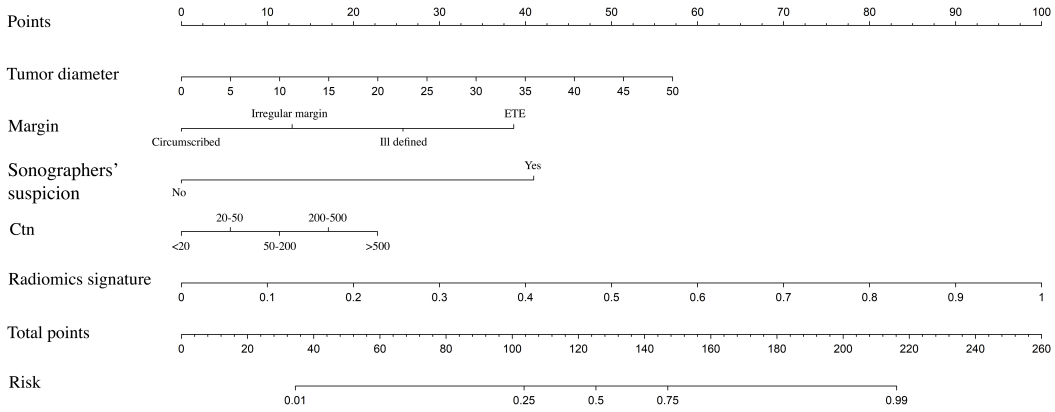

Fig. 7. Nomogram of the combined model for preoperative prediction of cervical LNM in MTC patients. Abbreviations: Ctn, calcitonin; LNM, lymph node metastasis; MTC, medullary thyroid carcinoma.

Discussion

Multiple studies have demonstrated that radiomics techniques utilizing primary tumour images offer effective strategies for predicting LNM, especially when combined with clinically independent predictors (Tan et al, 2020; Tong et al, 2021; Zhao et al, 2023). In this work, we used preoperative ultrasound images to create and validate a radiomics model to determine if patients with MTC had metastatic lymph nodes (LNs) in their cervical regions. The results showed that the clinical, radiomics, and combined models can preoperatively predict LNM in MTC patients (training dataset AUC: 0.800, 0.881, 0.925; validation dataset AUC: 0.805, 0.859, 0.918). The combined model outperformed the clinical and radiomics models in terms of accuracy and AUC, demonstrating higher predictive performance. The calibration curve analysis and the Hosmer-Lemeshow test results indicated that the predictions of the combined model were closest to the actual occurrences. DCA further demonstrated that the combined model provided the highest clinical net benefit across specific threshold probability ranges (approximate ranges: 0–0.85 for training and 0.13–1.00 for validation), highlighting its clinical utility in supporting personalized treatment decision-making.

LASSO regression analysis identified 19 optimal radiomic features in the training dataset. Among these, two were based on gray-level co-occurrence matrix (GLCM), one on gray-level dependence matrix (GLDM), nine on gray-level size zone matrix (GLSZM), four on neighboring gray-tone difference matrix (NGTDM), and three on gray-level run length matrix (GLRLM). GLSZM-based features accounted for a significant proportion (9/19), highlighting their importance in assessing whether cervical LNs in MTC patients have metastasized. GLSZM quantifies the number of adjacent pixels with the same grayscale value, reflecting the tumour's internal complexity and texture coarseness. This quantitative analysis may relate to the echo uniformity and margin clarity in ultrasound images. Furthermore, among the positively correlated features selected by the LASSO regression model, the "LowGrayLevelRunEmphasis" had the highest coefficient. This feature measures the concentration and continuity of low gray-level regions in the image. Higher

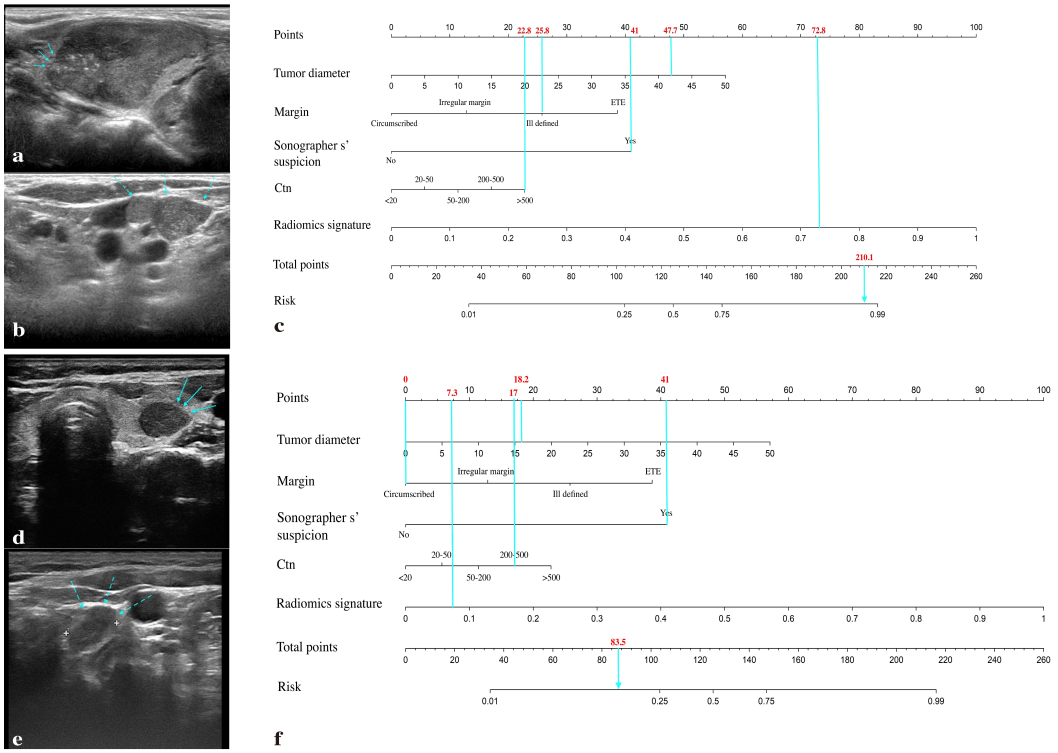

Fig. 8. Example of nomogram application. (a–c) Case 1. (d–f) Case 2. Note: Case 1: Case 1 represents a female patient bearing a tumour with a diameter of 42 mm on ultrasound examination and with ill-defined margin (indicated by the arrow in Fig. 8a), having a serum Ctn level of 1187.01 pg/mL, and who was suspected of harboring cervical LNM based on ultrasound findings (indicated by the arrow in Fig. 8b). The predicted probability by the radiomics model was 0.731. According to the nomogram for predicting cervical LNM in MTC patients in this study, the score was calculated as follows: 47.7 (tumour diameter 42 mm) + 25.8 (ill-defined margin) + 41 (sonographers' suspicion of cervical LNM based on ultrasound findings) + 22.8 (Ctn >500 pg/mL) + 72.8 (radiomics signature 0.731) = 210.1. The corresponding risk value for cervical LNM was 0.973 (Fig. 8c). Postoperative pathologic tests confirmed this case as cervical LNM-positive. Case 2: Case 2 represents a female patient carrying a tumour with a diameter of 16 mm on ultrasound examination and with circumscribed margin (indicated by the arrow in Fig. 8d), having a serum Ctn level of 209.62 pg/mL, and who was suspected of harboring cervical LNM based on ultrasound findings (indicated by the arrow in Fig. 8e). The predicted probability by the radiomics model was 0.072. According to the nomogram, the score was calculated as follows: 18.2 (tumour diameter 16 mm) + 0 (circumscribed margin) + 41 (sonographers' suspicion of cervical LNM based on ultrasound findings) + 17 (200 < Ctn < 500 pg/mL) + 7.3 (radiomics signature 0.072) = 83.5. The corresponding risk value for cervical LNM was 0.172 (Fig. 8f). Postoperative pathologic test confirmed this case as cervical LNM-negative.

values signify that these regions cover a larger area and are denser. This finding suggests that in tumour microenvironment analysis, concentrated low gray-level regions, such as necrotic tumour areas, are correlated with cervical LNM in MTC, consistent with the findings of Özer et al (2023). Dong et al (2023) found that the "SizeZoneNonUniformity" is an important feature for predicting metastasis in lateral neck LNs of papillary thyroid carcinoma (PTC). This feature is crucial for revealing tumour heterogeneity, as it reflects the non-uniformity of the size distribution within the tumour's internal structure, which may indicate irregular tumour

growth. Among the key features selected in this study, the "SizeZoneNonUniformity" appeared three times, indicating its unique value in revealing cervical LNM in MTC patients.

In addition to radiomics features, clinical features were also analyzed in this study. Univariate and multivariate logistic regression analyses performed on the training dataset identified four clinical independent predictors: tumour diameter, Ctn, margin, and sonographers' suspicion of cervical LNM based on ultrasound findings. The OR values for all the above clinical features are greater than 1, indicating that they are associated with an increased risk of cervical LNM in MTC patients. Clinical baseline data showed that patients with larger tumour diameters had a significantly higher rate of cervical LNM than those with smaller ones. This conclusion generally aligns with Esfandiari et al (2014), possibly because larger tumours grow faster or exist for a longer period, allowing more opportunities for spread to surrounding tissues or the lymphatic system. Additionally, larger tumours might compress or invade surrounding lymphatic vessels, aiding cancer cell spread. Among the patients with cervical LNM, 71.62% had Ctn levels >500 pg/mL, suggesting that high Ctn levels might serve as an important indicator, similar to the finding reported by Xu et al (2018). Luo et al (2022) pointed out that tumour margin, sonographers' suspicion of cervical LNM based on ultrasound findings, and extrathyroidal extension (ETE) were associated with cervical LNM in MTC patients. Their findings were corroborated by the current study but ETE features were integrated in the present study into the evaluation of tumour margin features based on the "2020 Chinese Thyroid Nodule Ultrasound Malignancy Risk Stratification Guidelines" (Zhou et al, 2020). Specifically, tumour margin can be categorized into four types: circumscribed, irregular, ill-defined, and ETE, where ETE refers to thyroid cancer cells breaking through the thyroid capsule and invading surrounding tissues. Aside from optimizing the diagnostic criteria, including ETE in the evaluation of tumour margin features provides a more accurate depiction of the interaction between the tumour and adjacent tissues, and reduces biases due to personal experience. In addition, this study revealed that sonographers' suspicion of cervical LNM based on ultrasound findings stands as a clinical independent predictor for cervical LNM in MTC patients, highlighting the critical role of experienced sonographers in detecting cervical LNM.

This study employed a creative approach to investigate and assess the application of ultrasound radiomics in determining whether cervical LNs in MTC patients have metastasized. However, there are certain limitations that need to be addressed:

(1) The application of the models cannot be translated to other settings or scenarios due to the small sample size and the single-center data used to create the models. A lack of external validation, owing to the low incidence rate of MTC, also undermines the generalizability of the models.

(2) Subjective judgement and bias in the collection process of clinical features and ultrasound images may affect the accuracy and stability of the model.

(3) This study did not consider other potential factors such as smoking and alcohol consumption, which could influence risk assessment, thus limiting the comprehensiveness of the risk assessment.

(4) Instead of utilizing both transverse and longitudinal plane images or multi-modal image fusion techniques, only one transverse plane ultrasound image of MTC was used to extract radiomic features. This could limit the comprehensive assessment and in-depth analysis of MTC features.

(5) In this study, sporadic and hereditary MTCs were not differentiated, nor were the specific locations of cervical LNs (central and lateral zones) considered in analysis, thus potentially influencing the accuracy of the model's predictions.

To address these issues, future studies should adopt a multi-center study design, expand the sample size, employ more comprehensive data (including genetic information and the location of metastatic LNs, etc.), use high-resolution ultrasonography, integrate ultrasound images viewed from different planes using more advanced deep learning methods, and employ multimodal fusion techniques for more accurate and reliable results.

Conclusion

The ultrasound-based radiomics model can preoperatively predict cervical LNM in MTC patients, but comparatively, the combined model, which integrates clinical independent predictors into radiomics model, demonstrates even better predictive performance.

Key Points

- Radiomics technology provides more detailed and rich information compared to traditional imaging analysis. This is an innovative attempt in the prediction of MTC.
- This study screened multiple clinical indicators and combined radiomics features with clinical characteristics to construct more comprehensive predictive models, demonstrating the potential of multi-source data fusion in improving prediction accuracy.
- This study enriches the existing literature about MTC, showcasing the high practical value of the conceived predictive models in clinical settings.

Availability of Data and Materials

The data that support the findings of this study are available on request from the corresponding authors, upon reasonable request.

Author Contributions

QL, FF and ML designed the research study. QL and FF conducted the research. QL and XZ analyzed the data. QL drafted the manuscript. FF, WZ, XZ, and ML revised the manuscript. WZ provided the data. All authors contributed to important editorial changes in the manuscript. All authors read and approved the

final manuscript. All authors have participated sufficiently in the work and agreed to be accountable for all aspects of the work.

Ethics Approval and Consent to Participate

The study received approval from the Ethics Committee of Ruijin Hospital, Shanghai Jiao Tong University School of Medicine (Ethics Review No.: 2024-320). Since the study was retrospective, the requirement for patient informed consent was exempted by the Ethics Committee of Ruijin Hospital, Shanghai Jiao Tong University School of Medicine.

Acknowledgement

Not applicable.

Funding

This research received no external funding.

Conflict of Interest

The authors declare no conflict of interest.

References

Baud G, Jannin A, Marciniak C, Chevalier B, Do Cao C, Leteurtre E, et al. Impact of Lymph Node Dissection on Postoperative Complications of Total Thyroidectomy in Patients with Thyroid Carcinoma. Cancers. 2022; 14: 5462. https://doi.org/10.3390/cancers14215462

Cui M, Zhang DY. Artificial intelligence and computational pathology. Laboratory Investigation. 2021; 101: 412–422. https://doi.org/10.1038/s41374-020-00514-0

Dong L, Han X, Yu P, Zhang W, Wang C, Sun Q, et al. CT Radiomics-Based Nomogram for Predicting the Lateral Neck Lymph Node Metastasis in Papillary Thyroid Carcinoma: A Prospective Multicenter Study. Academic Radiology. 2023; 30: 3032–3046. https://doi.org/10.1016/j.acra.2023.03.039

Duval MADS, Ferreira CV, Marmitt L, Dora JM, Espíndola M, Benini AF, et al. An Undetectable Postoperative Calcitonin Level Is Associated with Long-Term Disease-Free Survival in Medullary Thyroid Carcinoma: Results of a Retrospective Cohort Study. Thyroid. 2023; 33: 82–90. https://doi.org/10.1089/thy.2022.0295

Esfandiari NH, Hughes DT, Yin H, Banerjee M, Haymart MR. The effect of extent of surgery and number of lymph node metastases on overall survival in patients with medullary thyroid cancer. The Journal of Clinical Endocrinology and Metabolism. 2014; 99: 448–454. https://doi.org/10.1210/jc.2013-2942

Fan W, Xiao C, Wu F. Analysis of risk factors for cervical lymph node metastases in patients with sporadic medullary thyroid carcinoma. The Journal of International Medical Research. 2018; 46: 1982–1989. https://doi.org/10.1177/0300060518762684

Fugazzola L. Medullary thyroid cancer - An update. Best Practice & Research. Clinical Endocrinology & Metabolism. 2023; 37: 101655. https://doi.org/10.1016/j.beem.2022.101655

Hu XL, Ran HT. Ultrasound Radiomics Evaluation of Cervical Lymph Node Metastasis in Papillary Thyroid Carcinoma. Chinese Journal of Ultrasound in Medicine. 2022; 38: 367–370. (In Chinese)

Kandil E, Gilson MM, Alabbas HH, Tufaro AP, Dackiw A, Tufano RP. Survival implications of cervical lymphadenectomy in patients with medullary thyroid cancer. Annals of Surgical Oncology. 2011; 18: 1028–1034. https://doi.org/10.1245/s10434-010-1363-y

Konstantinidis A, Stang M, Roman SA, Sosa JA. Surgical management of medullary thyroid carcinoma. Updates in Surgery. 2017; 69: 151–160. https://doi.org/10.1007/s13304-017-0443-y

Kuo EJ, Sho S, Li N, Zanocco KA, Yeh MW, Livhits MJ. Risk Factors Associated With Reoperation and Disease-Specific Mortality in Patients With Medullary Thyroid Carcinoma. JAMA Surgery. 2018; 153: 52–59. https://doi.org/10.1001/jamasurg.2017.3555

Li C, Zheng M, Zheng X, Fang X, Dong J, Wang C, et al. Predictive Ki-67 Proliferation Index of Cervical Squamous Cell Carcinoma Based on IVIM-DWI Combined with Texture Features. Contrast Media & Molecular Imaging. 2021; 2021: 8873065. https://doi.org/10.1155/2021/8873065

Luo Z, Hong Y, Yan C, Ye Q, Wang Y, Huang P. Nomogram for preoperative estimation risk of cervical lymph node metastasis in medullary thyroid carcinoma. Frontiers in Oncology. 2022; 12: 883429. https://doi.org/10.3389/fonc.2022.883429

Machens A, Dralle H. Biomarker-based risk stratification for previously untreated medullary thyroid cancer. The Journal of Clinical Endocrinology & Metabolism. 2010; 95: 2655–2663. https://doi.org/10.1210/jc.2009-2368

Özer H, Batur A, Özdemir N, Durmaz MS, Kılınçer A. Magnetic Resonance Imaging Texture Analysis in the Detection of Metastatic Lymph Nodes in Patients with Nasopharyngeal Carcinoma. Genel Tıp Dergisi. 2023; 33: 461–465. https://doi.org/10.54005/geneltip.1311577

Park VY, Han K, Kim HJ, Lee E, Youk JH, Kim EK, et al. Radiomics signature for prediction of lateral lymph node metastasis in conventional papillary thyroid carcinoma. PLoS ONE. 2020; 15: e0227315. https://doi.org/10.1371/journal.pone.0227315

Randle RW, Balentine CJ, Leverson GE, Havlena JA, Sippel RS, Schneider DF, et al. Trends in the presentation, treatment, and survival of patients with medullary thyroid cancer over the past 30 years. Surgery. 2017; 161: 137–146. https://doi.org/10.1016/j.surg.2016.04.053

Shen B, Zhou C, Xu C, Yang B, Wu X, Fu X, et al. Ultrasound-based Radiomics for Predicting Metastasis in the Lymph Nodes Posterior to the Right Recurrent Laryngeal Nerve in Patients with Papillary Thyroid Cancer. Current Medical Imaging. 2024; 20: 1–11. https://doi.org/10.2174/0115734056257332231024112410

Siironen P, Hagström J, Mäenpää HO, Louhimo J, Arola J, Haglund C. Lymph node metastases and elevated postoperative calcitonin: Predictors of poor survival in medullary thyroid carcinoma. Acta Oncologica. 2016; 55: 357–364. https://doi.org/10.3109/0284186X.2015.1070963

Tan H, Gan F, Wu Y, Zhou J, Tian J, Lin Y, et al. Preoperative Prediction of Axillary Lymph Node Metastasis in Breast Carcinoma Using Radiomics Features Based on the Fat-Suppressed T2 Sequence. Academic Radiology. 2020; 27: 1217–1225. https://doi.org/10.1016/j.acra.2019.11.004

Temizhan E, Mirtagioglu H, Mendes M. Which correlation coefficient should be used for investigating relations between quantitative variables. American Academic Scientific Research Journal for Engineering, Technology, and Sciences. 2022; 85: 265–277. https://asrjetsjournal.org/index.php/American_Scientific_Journal/article/view/7326/2499

Thomas CM, Asa SL, Ezzat S, Sawka AM, Goldstein D. Diagnosis and pathologic characteristics of medullary thyroid carcinoma-review of current guidelines. Current Oncology. 2019; 26: 338–344. https://doi.org/10.3747/co.26.5539

Tong Y, Li J, Huang Y, Zhou J, Liu T, Guo Y, et al. Ultrasound-Based Radiomic Nomogram for Predicting Lateral Cervical Lymph Node Metastasis in Papillary Thyroid Carcinoma. Academic Radiology. 2021; 28: 1675–1684. https://doi.org/10.1016/j.acra.2020.07.017

van Beek DJ, Almquist M, Bergenfelz AO, Musholt TJ, Nordenström E. Complications after medullary thyroid carcinoma surgery: multicentre study of the SQRTPA and EUROCRINE® databases. The British Journal of Surgery. 2021; 108: 691–701. https://doi.org/10.1093/bjs/znaa195

van den Heuvel E, Zhan Z. Myths about linear and monotonic associations: Pearson'sr, Spearman's ρ, and Kendall's τ. The American Statistician. 2022; 76: 44–52. https://doi.org/10.1080/00031305.2021.2004922

Wang W, Peng Y, Feng X, Zhao Y, Seeruttun SR, Zhang J, et al. Development and validation of a computed tomography–based radiomics signature to predict response to neoadjuvant chemotherapy for locally advanced gastric cancer. JAMA Network Open. 2021; 4: e2121143.

https://doi.org/10.1001/jamanetworkopen.2021.21143

Wang XB, Ju HY, Sun LY, Chen N. Analysis of the Impact of Immunohistochemical Staining on Quality Control in Pathological Techniques. Guizhou Medical Journal. 2023; 47: 1461–1463. (In Chinese)

Wells SA, Jr, Asa SL, Dralle H, Elisei R, Evans DB, Gagel RF, et al. Revised American Thyroid Association Guidelines for the Management of Medullary Thyroid Carcinoma: The American Thyroid Association Guidelines Task Force on Medullary Thyroid Carcinoma. Thyroid. 2015; 25: 567–610. https://doi.org/10.1089/thy.2014.0335

Wen Q, Wang Z, Traverso A, Liu Y, Xu R, Feng Y, et al. A radiomics nomogram for the ultrasound-based evaluation of central cervical lymph node metastasis in papillary thyroid carcinoma. Frontiers in Endocrinology. 2022; 13: 1064434. https://doi.org/10.3389/fendo.2022.1064434

Wu L, Zhao Y, Lin P, Qin H, Liu Y, Wan D, et al. Preoperative ultrasound radiomics analysis for expression of multiple molecular biomarkers in mass type of breast ductal carcinoma in situ. BMC Medical Imaging. 2021; 21: 84. https://doi.org/10.1186/s12880-021-00610-7

Xu N, Jian Y, Wang Y, Tian W. Evaluation of neutrophil-to-lymphocyte ratio and calcitonin concentraion for predicting lymph node metastasis and distant metastasis in patients with medullary thyroid cancer. Molecular and Clinical Oncology. 2018; 9: 629–634. https://doi.org/10.3892/mco.2018.1727

Zhang Y, Wang K, Liu J, Xu S, Sun Y, Xu M, et al. Surgical management of parapharyngeal lymph node metastases from thyroid carcinoma with transcervical approach. Surgery. 2022; 171: 1233–1239. https://doi.org/10.1016/j.surg.2021.08.054

Zhao J, Yang F, Wei X, Mao Y, Mu J, Zhao L, et al. Ultrasound features value in the diagnosis and prognosis of medullary thyroid carcinoma. Endocrine. 2021; 72: 727–734. https://doi.org/10.1007/s12020-020-02510-2

Zhao X, Li W, Zhang J, Tian S, Zhou Y, Xu X, et al. Radiomics analysis of CT imaging improves preoperative prediction of cervical lymph node metastasis in laryngeal squamous cell carcinoma. European Radiology. 2023; 33: 1121–1131. https://doi.org/10.1007/s00330-022-09051-4

Zhou J, Yin L, Wei X, Zhang S, Song Y, Luo B, et al. 2020 Chinese guidelines for ultrasound malignancy risk stratification of thyroid nodules: the C-TIRADS. Endocrine. 2020; 70: 256–279. https://doi.org/10.1007/s12020-020-02441-y

Zhu XL, Luo XL, Wu HM, Yao J, Lin XT, Dou WX. Quality Control in the Handling of Pathological Tissue Specimens. Chinese Journal of Clinical and Experimental Pathology. 2019; 35: 1249–1250. (In Chinese)